AIAA 99 - 2189

NUMERICAL PREDICTION OF TRANSIENT AXIAL THRUST AND INTERNAL FLOWS IN A ROCKET ENGINE TURBOPUMP

Katherine Van Hooser
Marshall Space Flight Center
Huntsville, Alabama

and

John Bailey and Alok Majumdar
Sverdrup Technology, Inc.
Huntsville, Alabama

35th AIAA/ASME/SAE/ASEE Joint Propulsion Conference and Exhibit
20-24 June 1999
Los Angeles, California

AIAA-99-2189

NUMERICAL PREDICTION OF TRANSIENT AXIAL THRUST AND INTERNAL FLOWS IN A ROCKET ENGINE TURBOPUMP

Katherine Van Hooser
Marshall Space Flight Center
Huntsville, Alabama 35812

John Bailey & Alok Majumdar
Sverdrup Technology, MSFC Group
Huntsville, Alabama 35806

ABSTRACT

This paper presents a numerical model of internal flows in a rocket engine turbopump developed with the Generalized Fluid System Simulation Program, GFSSP. The axial thrust and internal flow distribution of the Fastrac turbopump were calculated during the start transient of a component test. GFSSP computes the time-dependant flow in the internal or secondary flow circuits of the turbopump for the Fastrac engine that is currently under development at Marshall Space Flight Center. GFSSP is a general-purpose computer program for analyzing steady state and time-dependant flowrates, pressures, temperatures, and concentrations in a complex flow network. The program employs a finite volume formulation of mass, momentum, and energy conservation equations in conjunction with the thermodynamic equation of state of real fluids. Predicted results were then compared with pressures and temperatures recorded during the test. Most of the comparisons showed good agreement.

NOMENCLATURE

A	Cross-Sectional Area (ft^2)
c	Concentration of Specie in Mixture
g	Gravitational Acceleration (ft/sec^2)
g_c	Conversion Constant (=32.174 lb_m-ft/lb_f -sec^2)
J	Mechanical Equivalent of Heat (778 ft-lb_f /Btu)
K_f	Flow Resistance Coefficient (lb_f -sec^2 /$lb_m{}^2$-ft^2)
K_{rot}	Non-dimensional Rotating Flow Resistance Coefficient
m	Resident Mass (lb_m)
$\dot{m}$	Mass Flow Rate (lb_m/sec)
n	Number of Branches
p	Pressure (lb_f / ft^2)
Q	Heat Source (Btu/sec)
r	Radius (ft)
S	Momentum Source(lb_f)
$\dot{S}_{gen}$	Entropy Generation Rate (Btu/°R-sec)
s	Entropy (Btu/lbm - °R)
T	Temperature (°R)
u	Velocity (ft/s)
V	Volume (ft^3)

Greek

ρ	Density (lb_m/ft^3)
θ	Angle Between Branch Flow Velocity Vector and Gravity Vector (deg)
ω	Angular Velocity (rad/sec)
$\Delta\tau$	Time Step (sec)
τ	Time (sec)

Subscript

i	i^{th} Node
j	j^{th} Node
k	Fluid Specie
ij	Branch connecting i^{th} and j^{th} Node
u	Upstream Node

INTRODUCTION

Accurate predictions of the pressure distribution in the secondary flow path (through bearings and seals) as well as the primary flow path (through inducer, impeller, or turbine blades) are important to the turbopump designer. Secondary flow path calculations may be used to ensure that the bearing coolant flows are adequate, that overboard leakage is minimal, that separation of the oxidizer and fuel is maintained, and

that the net axial thrust is within the capability of the bearings.

Predicting the secondary flow distribution in a liquid rocket engine turbopump requires modeling fluid flow in a very complex network. Such a network involves flow through extremely narrow passages, flow between rotating and stationary surfaces, phase changes, mixing of fluids, and heat transfer. Available commercial codes[1-2] are generally suitable for steady state, single phase, incompressible flow. Because of the proprietary nature of such codes, it is not possible to extend their capability to satisfy the above-mentioned needs.

In the past, specific purpose codes[3-4] were developed to model the Space Shuttle Main Engine (SSME) turbomachinery. However, it was difficult to use those codes for a new design without making extensive changes in the original codes. Such efforts often turn out to be time consuming and inefficient. Majumdar and Van Hooser[5] described a finite volume procedure to model steady state flow distribution, pressures, temperatures, and concentrations of mixtures in complex flow circuits. Their predictions compared well with Pratt & Whitney's predictions of internal flows in the SSME Alternate High Pressure Oxidizer Turbopump.

The finite volume procedure was incorporated into a general-purpose computer program called the Generalized Fluid System Simulation Program[6] (GFSSP). The GFSSP steady state predictions for the Simplex[7-8] turbopump compared well with test data. The finite volume formulation of GFSSP was further extended[9] to model transient flow to predict time-dependant flow characteristics. This paper presents the application of the GFSSP to predict the time-dependant flow in a complex secondary flow circuit of the Fastrac turbopump currently under development at Marshall Space Flight Center (MSFC).

MATHEMATICAL FORMULATION

The analysis of the flow distribution in a complex flow network requires modeling of the system using boundary nodes, internal nodes, and branches. At boundary nodes pressures, temperatures, and concentrations are prescribed. At internal nodes pressures, temperatures, and concentrations are computed by solving time-dependant mass, energy, and specie conservation equations. The time-dependant momentum conservation equations are solved in all branches to compute flowrates.

Figure 1 displays a schematic showing adjacent nodes, their connecting branches, and the indexing system used by GFSSP.

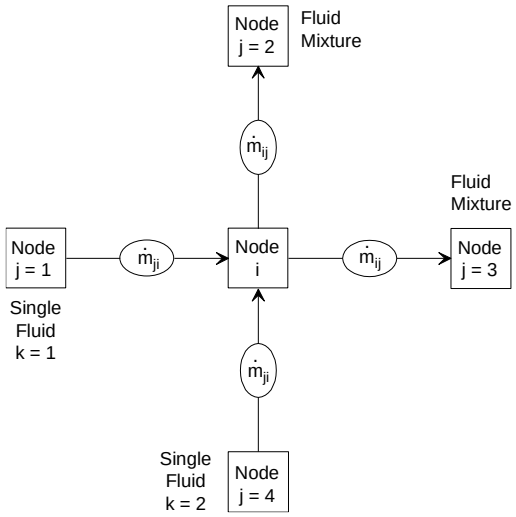

Figure 1 - Schematic of GFSSP Nodes, Branches, and Indexing Practice

Mass Conservation Equation

The mass conservation equation at the i^{th} node can be expressed as:

$$\frac{(m_i)_{\tau+\Delta\tau} - (m_i)_{\tau}}{\Delta\tau} = \sum_{j=1}^{j=n} \dot{m}_{ij} \qquad (1)$$

Equation 1 requires that, for the transient formulation, the net mass flow from a given node must equate to the rate of change of mass in the control volume.

Energy Conservation Equation

The energy conservation equation for node i, is expressed in terms of entropy by:

$$\frac{(m_i s_i)_{\tau+\Delta\tau} - (m_i s_i)_{\tau}}{\Delta\tau} =$$

$$\sum_{j=1}^{j=n} \left\{ MAX\left[-\dot{m}_{ij}, 0\right] s_j - MAX\left[\dot{m}_{ij}, 0\right] s_i \right\} + \qquad (2)$$

$$\sum_{j=1}^{j=n} \left\{ \frac{MAX\left[-\dot{m}_{ij}, 0\right]}{\left|\dot{m}_{ij}\right|} \right\} \dot{S}_{ij,\,gen} + \frac{Q_i}{T_i}$$

The entropy generation rate due to fluid friction in a branch is expressed as:

$$\dot{S}_{ij,\,gen} = \frac{\dot{m}_{ij}\Delta p_{ij,viscous}}{\rho_u T_u J} = \frac{K_f\left(\left|\dot{m}_{ij}\right|\right)^3}{\rho_u T_u J} \qquad (2a)$$

The MAX operator in Equation 2 reflects the use of an upwind differencing scheme. When the flow direction is not known, this operator allows the transport of entropy only from its upstream neighbor. In other words, the upstream neighbor influences its downstream neighbor but not vice-versa. The first term on the right side of the equation represents the convective transport of entropy from neighboring nodes. The second term represents the rate of entropy generation in branches connected to the i[th] node. The third term represents the entropy change due to heat transfer.

Specie Conservation Equation

GFSSP has been developed to handle either pure fluids or mixtures. For mixtures, the concentration of fluid specie must be determined so that the density may be calculated. The concentration for the k[th] specie at node i is:

$$\frac{\left(m_i c_{i,k}\right)_{\tau+\Delta\tau} - \left(m_i c_{i,k}\right)_{\tau}}{\Delta\tau} = \sum_{j=1}^{j=n}\left\{MAX\left[-\dot{m}_{ij},0\right]c_{j,k} - MAX\left[\dot{m}_{ij},0\right]c_{i,k}\right\} \qquad (3)$$

Momentum Conservation Equation

The flow rate in a branch is calculated from the momentum conservation equation (Equation 4) which represents the balance of fluid forces acting on a given branch. A typical branch configuration is shown in Figure 2. Inertia, pressure, gravity, friction, and centrifugal forces are considered in the conservation equation. In addition to these five forces, a source term S has been provided in the equation to input pump characteristics or to input the power of a pump in a given branch. If a pump is located in a given branch, all of the other forces in that branch, except for pressure, are set to zero. The source term, S, is set to zero in all branches without a pump. It should also be noted that the flowrate, $\dot{m}_{ij}$, is a vector quantity. A negative value of $\dot{m}_{ij}$ signifies that the flow is directed from the j[th] node to the i[th] node.

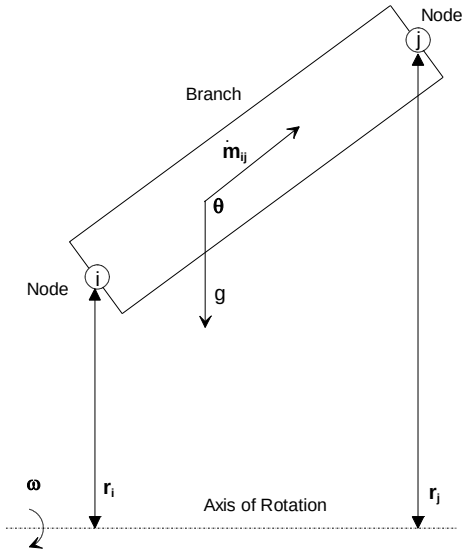

Figure 2 - Schematic of a Branch Showing Rotation

$$\frac{\left(m_{ij}u_{ij}\right)_{\tau+\Delta\tau} - \left(m_{ij}u_{ij}\right)_{\tau}}{\Delta\tau} + \frac{\dot{m}_{ij}}{g_c}\left(u_{ij} - u_u\right) = \left(p_i - p_j\right)\mathrm{A_{ij}} + \frac{\rho_u g V_{ij}\cos\theta}{g_c} - K_f\dot{m}_{ij}\left|\dot{m}_{ij}\right|\mathrm{A_{ij}} + \frac{\rho_u K_{rot}^2\omega^2}{2g_c}\mathrm{A_{ij}}\left(r_j^2 - r_i^2\right) + S_{ij} \qquad (4)$$

The two terms on the left side of the momentum equation represent the inertia of the fluid. The first term is the time dependent term which must be considered for unsteady calculations. The second term is significant when there is a large change in area or density from branch to branch. The first term on the right side of the momentum equation represents the pressure gradient in the branch. The second term represents the effect of gravity. The gravity vector makes an angle (θ) with the assumed flow direction vector. The third term represents the frictional effect. Friction is modeled as a product of K_f, the square of the flow rate, and area. K_f is a function of the fluid density in the branch and the nature of flow passage being modeled by the branch. The fourth term in the momentum equation represents the effect of the centrifugal force. This term will be present only when the branch is rotating as shown in Figure 2. K_{rot} in this term is a factor representing fluid rotation and is unity when the fluid and the surrounding solid surface rotate at the same speed. This term also requires the radial distances from the upstream and downstream faces of the branch to the axis of rotation. The details of the numerical solution procedure and computer program are described in Reference 9.

FASTRAC TURBOPUMP CONFIGURATION AND GFSSP MODEL

The Fastrac engine is a 60,000-lbf thrust LOX and RP-1 engine being developed for the X-34 vehicle by MSFC. When the Fastrac turbopump (Figure 3) was being designed, GFSSP was used to predict the steady-state internal flows and net axial thrust. This turbopump has since been tested at MSFC. Data from this testing program has been used to validate the transient capabilities of GFSSP.

The turbopump consists of a fuel (RP-1) pump and oxidizer (LOX) pump that are connected by a common shaft, which is driven by a turbine. Internal fuel and oxidizer seal leakage flows are separated by the Inter-Propellant Seal (IPS) package which uses helium as a buffer fluid.

GFSSP Model of the Fastrac Turbopump

The overall configuration of the Fastrac turbopump GFSSP model structure is shown in Figure 4. The turbopump model consists of 11 boundary nodes, 39 internal nodes, and 72 branches.

A partial cross-section of the turbopump appears in Figure 5 to relate the nodal locations from Figure 4 to the LOX pump hardware, though only a few nodes are labeled. LOX leaving the impeller discharge (node 110) leaks around both the front and back of the impeller. The front-face leakage travels radially inward (branch 409), crosses a 4-tooth labyrinth seal (branch 401), and returns to the impeller inlet (node 102). The back-face leakage travels radially inward through eight rotating vanes (branch 410), cools the bearing (branch 413) and then splits. The majority of the flow returns through two external return lines (branches 4321-4331 and 4322-4332) to the inducer inlet (node

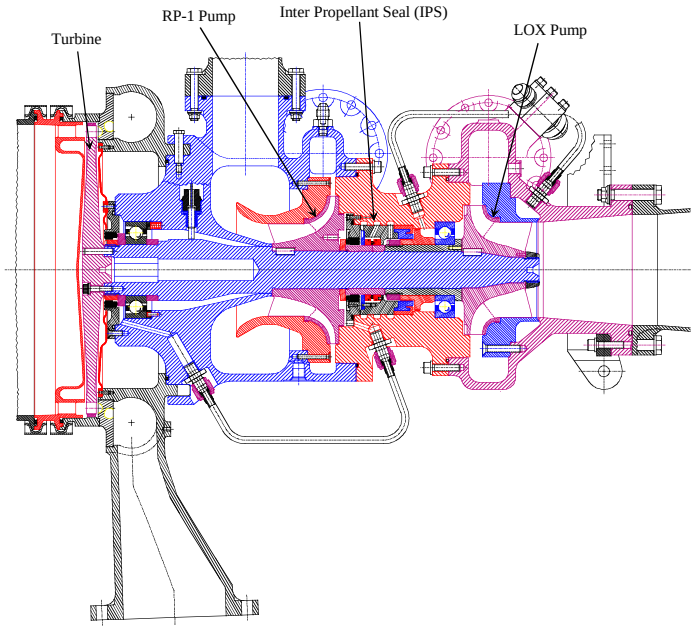

Figure 3 - Fastrac Turbopump Geometry

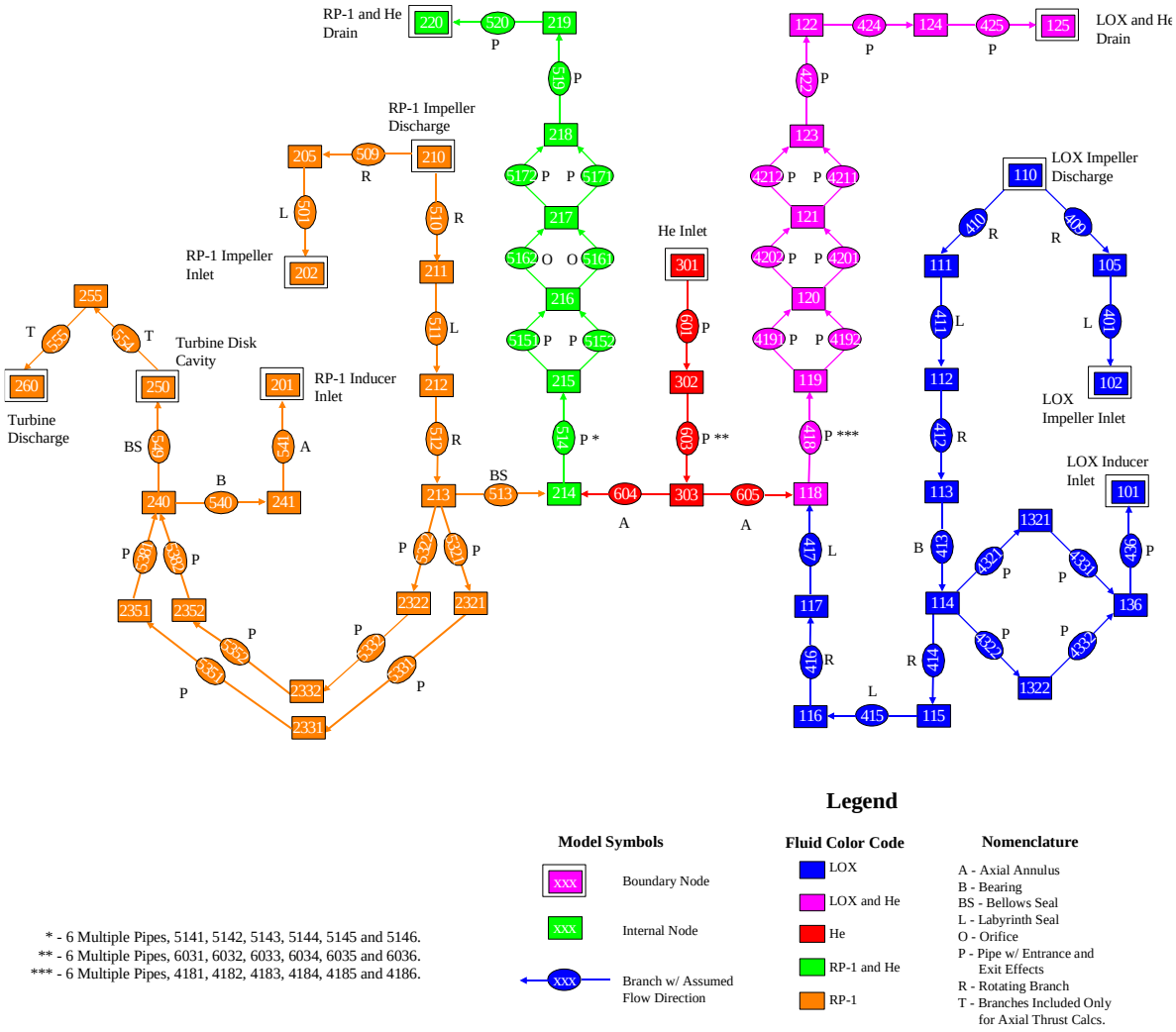

Figure 4 - Overall GFSSP Model Structure

101). The remainder of the flow travels across a 5-tooth labyrinth seal (branch 415) and a 9-tooth labyrinth seal (branch 417) before mixing with the IPS purge gas at node 118. Helium enters the turbopump at node 301 and splits, crossing two shaft-riding carbon seals at branches 604 and 605. The LOX and helium mixture then drains overboard (nodes 118-125).

Early Fastrac turbopump GFSSP models included a constant heat load at node 113 to simulate the heat added to the fluid by the LOX pump bearing. It was discovered that this heat load had very little impact on the flow field but that it contributed significantly to numerical instabilities, due to fluid phase changes during the iterative process, so it was omitted from successive models. Before the design was final, a labyrinth seal was located on the back-face of the LOX impeller. Because axial thrust in the direction of the LOX impeller had to be decreased, the labyrinth seal was replaced with 8 rotating vanes. The seal resistance (branch 411) was left in the model, but the modeled seal clearance was increased to eliminate the pressure drop in this branch. The resistance therefore no longer influences the rest of the flow circuit.

The fuel pump and turbine side of the turbopump is shown in Figure 6 so that nodal locations from Figure 4 may be related to the hardware, though only a few of the nodes are labeled. The fuel internal leakage paths are similar to those on the oxidizer side. RP-1 leaving the impeller discharge (node 210) leaks around both the front and back of the impeller. The front-face leakage travels radially inward (branch 509), crosses a 4-tooth labyrinth seal (branch 501), and returns to the impeller inlet (node 202). The back-face leakage travels radially inward (branch 510), crosses a 5-tooth labyrinth seal (branch 511), and then splits. A very small amount of flow crosses the bellows seal (branch 513), mixes with

the IPS purge and drains overboard (nodes 214-220). The majority of the back-face leakage travels through two external bearing coolant lines (branches 5321-5381 and 5322-5382) to the cavity (node 240) located between the turbine-end ball bearing and the turbine-end bellows seal. A small amount of this flow crosses the turbine-end bellows seal (branch 549) and exits the turbopump through turbine disk cavity (node 250) and the turbine blades (which are not included in the model). Most of the RP-1 leakage returns to the RP inducer inlet (node 201) through the bearing (branch 540) and a rotating annular duct (branch 541). A constant heat load is added at node 240 to simulate the heat transferred from the RP-1 pump bearing to the fluid.

An additional boundary node (260) was added to the model so that the force caused by the pressure on the downstream side of the turbine disk could be included in the summation of axial thrusts. An internal node (255) and two branches (555 & 554) also had to be added to connect the boundary nodes on the two sides of the turbine disk. The flow conditions at this internal node and in the two added branches have no effect on the rest of the flow circuit.

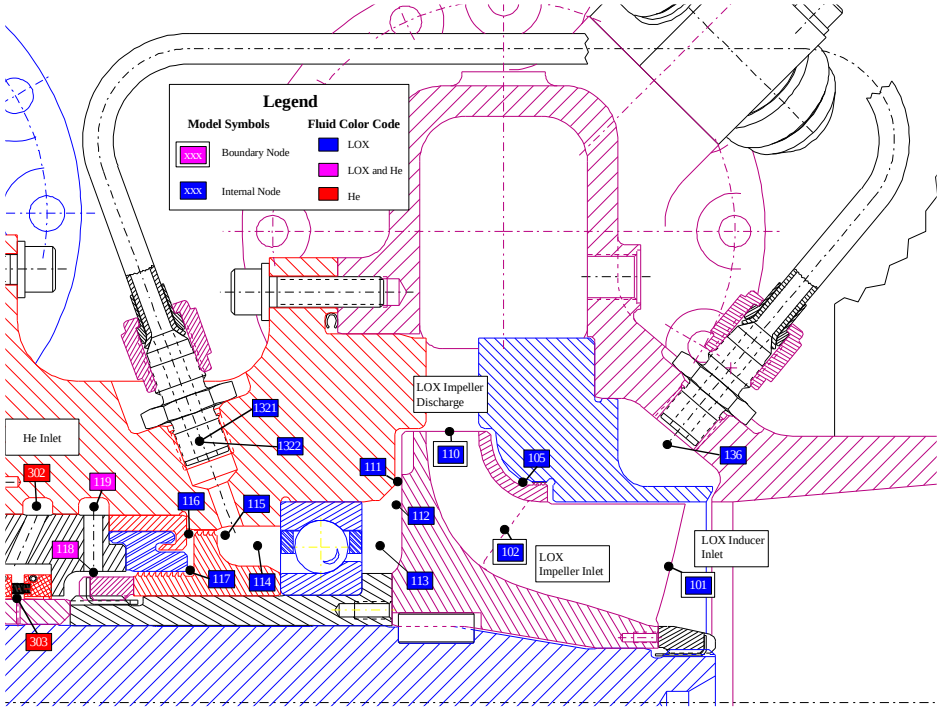

Figure 5 - Fastrac Turbopump LOX Internal Flow Paths

Boundary Conditions

The boundary conditions (Figures 7 - 9) for this transient model were derived from measured pressure and temperature data taken from a Fastrac turbopump component test conducted on March 2, 1999 at MSFC. The pump rotational speed has been included on the figures. Pump speed is required to compute the centrifugal force term in Equation 4. Since pressures and temperatures were not measured at locations comparable to all of the boundary node locations, some of the boundary condition data had to be calculated. Inducer inlet pressures and temperatures were measured and used as boundary conditions for both pumps. Inducer and impeller discharge pressures for both pumps were calculated from inlet pressures, inlet flowrates, speed, and correlations developed during the design process using CFD (Computational Fluid Dynamics) analysis of the inducer and impeller flow passages. Temperatures were measured at both pump discharge flanges. It was assumed that the impeller discharge temperatures equaled the measured discharge flange temperatures. Inducer discharge temperatures were calculated by assuming that 20% of the pump temperature increase occurred in the inducers. Pressure data was recorded at locations corresponding to the model boundary nodes located in the turbine discharge cavity and the turbine disk cavity. The IPS helium supply was instrumented with temperature and pressure

sensors. The two IPS drain outlets were assumed to be at sea level atmospheric pressure and 70°F.

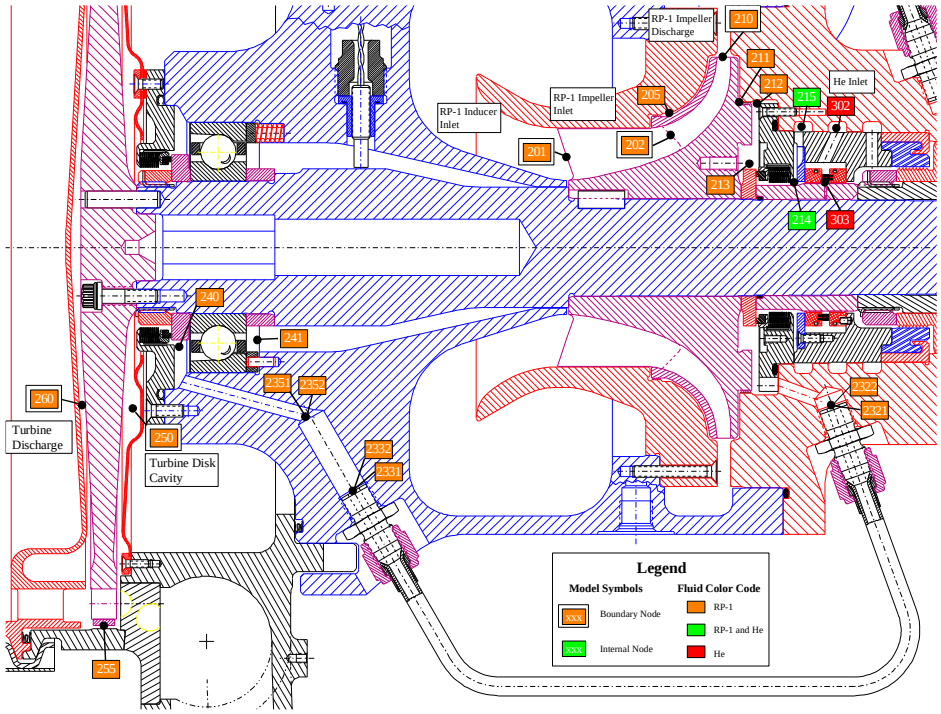

Figure 6 - Fastrac Turbopump RP-1 Internal Flow Paths

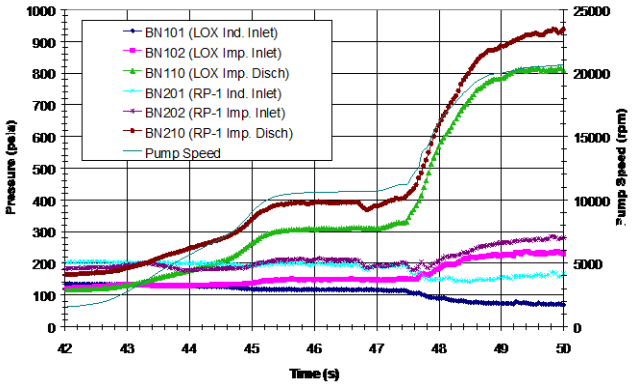

Figure 7 - Fastrac Turbopump Start Transient Model LOX and RP-1 Pump Boundary Pressures

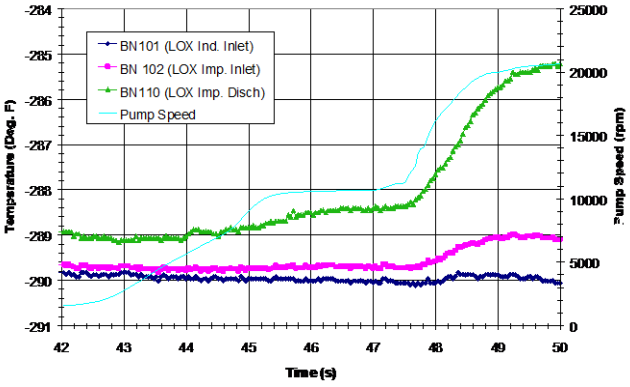

Figure 8 - Fastrac Turbopump Start Transient Model LOX Pump Boundary Temperatures

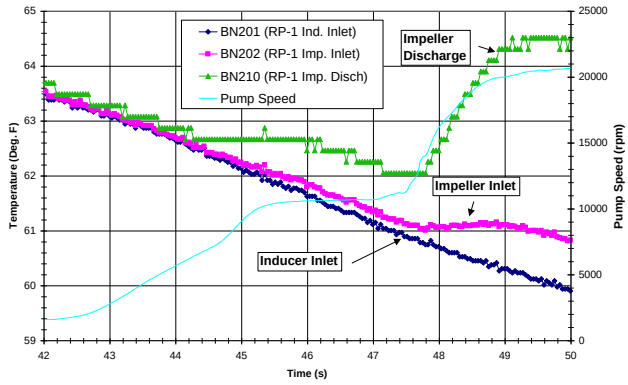

Figure 9 - Fastrac Turbopump Start Transient Model RP-1 Pump Boundary Temperatures

RESULTS

The axial thrust calculated by GFSSP during the start transient is shown in Figure 10. The assumed sign convention is that positive thrust acts in the direction of the oxidizer pump and a negative thrust acts in the direction of the turbine. To investigate the model sensitivity to the time increment used, two cases were run. One case used a time step of 0.5 seconds and the other used a time step of 0.1 seconds, except for a time period from 47.7 to 48.0 seconds where a time step of 0.3 seconds was used to overcome numerical convergence difficulties. It was decided during the design process that the desired net axial thrust at mainstage was approximately –1000 lbf, and that the axial thrust could acceptably range between -1500 and +500 lbf. As seen in the figure, GFSSP predicted start transient loads remain within the desired boundaries and that the mainstage level is relatively close to the desired value. It can also be seen in this figure that decreasing the time step results in increasing the resolution of the predicted results.

Modeling a component test of the Fastrac turbopump provided the opportunity to compare the GFSSP predicted flow field with measured pressures and temperatures. Figures 11 through 16 show comparisons between the GFSSP predictions and measured pressure and temperature data. Good agreement (within 10%) was observed between the test and predicted data except in the two IPS drains and downstream of the LOX pump bearing.

Figure 11 shows that the pressure recorded downstream of the LOX bearing is much lower than the prediction. Reasons for this discrepancy are unknown but may be related to the measurement location in the cavity. The bearing resistance was calculated using test data from similar bearings. The same assumptions were used in modeling the RP-1 bearing, which matches model predictions very well (Figure 14). Also, the same bearing was used in MSFC's Simplex turbopump, which was modeled using GFSSP[8]. Results from that model matched test data very well.

Figure 12 shows a good correlation between the predicted LOX bearing coolant return cavity pressure and the test data. Excellent agreement is shown in Figure 13 between the pressures predicted by GFSSP upstream and downstream from the RP-1 pump impeller back face labyrinth seal and the test data. Figure 15 shows a comparison between the predicted temperature downstream from the RP-1 bearing and the test data. Initially, this comparison shows a good correlation; however, due to modeling the bearing heat load as a constant value, the predicted temperature deviates from the test data toward the end of the start transient.

The predicted LOX drain pressure is significantly higher than the measured value (110 psia predicted versus 70 psia measured). The drain is long (approximately 80 inches), uninsulated, and thus is influenced by ambient heat transfer. The amount of drain line heat input modeled affects the location of the phase change for the LOX and helium mixture and therefore affects the pressure profile in the drain. Iterations with the steady-state model have shown that, once the model is anchored to data by changing the drain heat input, successive tests match predictions.

Pressure data recorded in the RP-1 drain during the test was significantly higher than predicted (Figure 16). A post-test disassembly revealed an unseated carbon ring in the bellows seal immediately upstream of the RP-1 drain. This seal, represented in the model by branch 513, controls the amount of overboard RP-1 leakage and therefore controls the RP-1 drain pressure. The unseated carbon ring probably increased the flow area through the seal, causing the high drain pressures measured in the test. Iterations with the steady-state GFSSP model have shown that the RP-1 drain pressure is extremely sensitive to the seal clearance or flow area used at branch 513. Previous tests with other turbopump builds have shown mainstage drain pressures of approximately 23 psia which compare more favorably with the corresponding GFSSP prediction of 35 psia.

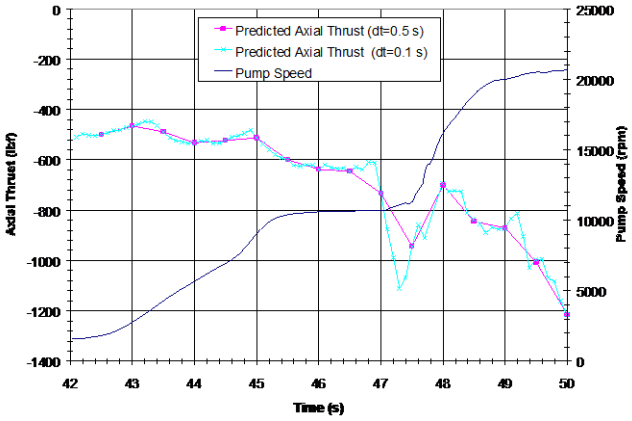

Figure 10 - GFSSP Predicted Axial Thrust During the Start Transient

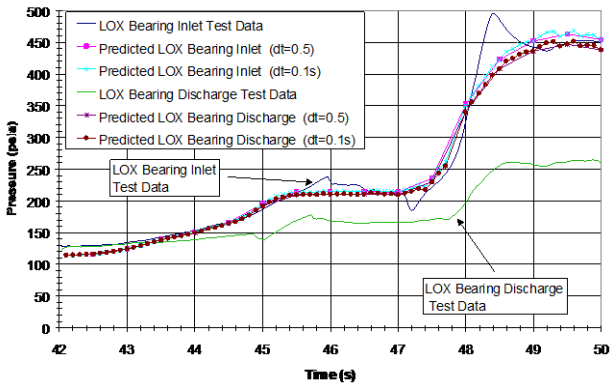

Figure 11 - Comparison of Test Data and Predicted LOX Bearing Inlet (Node 113) and Discharge (Node 114) Pressures

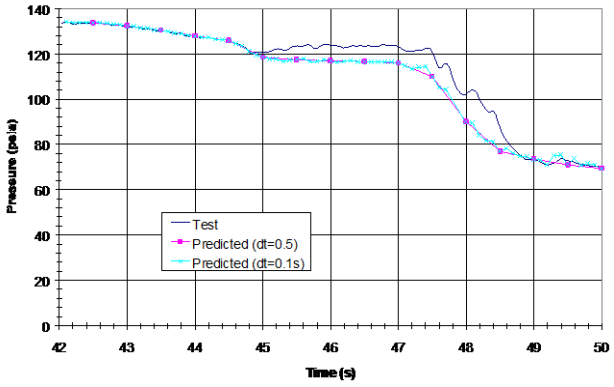

Figure 12 - Comparison of Test Data and Predicted LOX Bearing Coolant Return (Node 136) Pressure

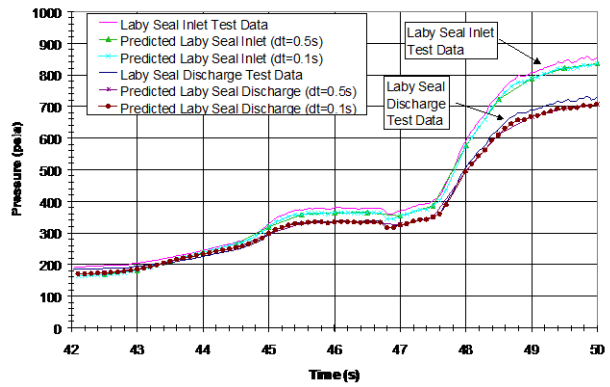

Figure 13 - Comparison of Test Data and Predicted RP-1 Impeller Back Face Labyrinth Seal Inlet (Node 211) and Discharge (Node 212) Pressure

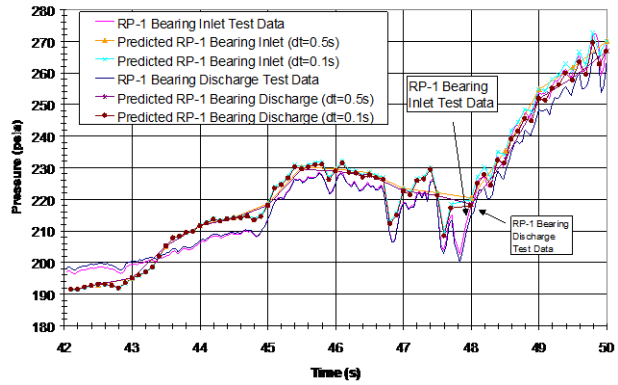

Figure 14 - Comparison of Test Data and GFSSP Predicted RP-1 Bearing Inlet (Node 240) and Discharge (Node 241) Start Transient Pressure

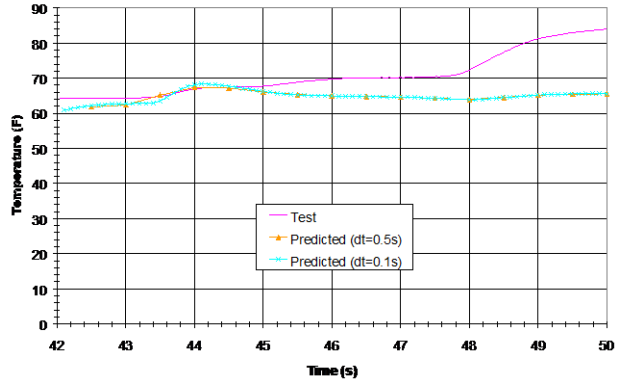

Figure 15 - Comparison of Test Data and Predicted RP-1 Bearing Discharge (Node 241) Start Transient Temperature

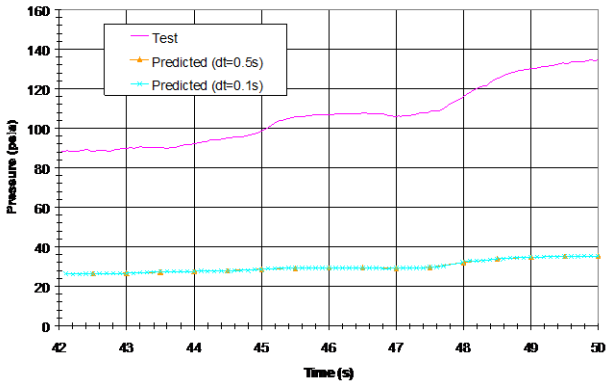

Figure 16 – Comparison of Test Data and Predicted RP-1 Drain Line (Node 215) Pressure

CONCLUSIONS

1. This paper describes a transient finite volume model of internal flows of the Fastrac turbopump. The model was developed with the Generalized Fluid System Simulation Program, GFSSP.
2. The model includes leakage flow from both oxidizer and fuel pump discharges, mixing of each of the propellants with helium in the Inter-Propellant Seal (IPS) package, disk rotation, and phase change.
3. The numerical predictions are compared with measured pressure and temperature data. Generally, a good agreement was observed between measurements and predictions. However, a significant discrepancy in pressures is observed in the LOX pump drain line. This discrepancy is attributed to the heat transfer from the ambient to the LOX. This conclusion was reached after performing several parametric studies with constant heat input in to the model. Future efforts will be directed to improve modeling of heat transfer from the surroundings.
4. The ability to predict axial thrust loads during the start transient provides an analytical capability that MSFC did not have previously.

ACKNOWLEDGEMENT

The work was performed under Task Directive 371-401 for MSFC Science and Engineering Contract NAS 8-40836 with Mr. Henry Stinson of Marshall Space Flight Center as Task Initiator. The authors would like to acknowledge Mr. Tom Beasley of Sverdrup Technology for his suggestions and review.

REFERENCES

1. Crane Company, "Flow of Fluids through Valves, Fittings and Pipe.", Technical Paper No. 410, 1988.
2. Kelix Software System, "Protopipe for Windows, Version 1.0", 1993-95
3. Anderson, P. G. et al, "Fluid Flow Analysis of the SSME High Pressure Oxidizer Turbopump Operating at Full Power Level", Lockheed Missiles & Space Company, Inc., Report No. LMSC-HREC TR D698083, Contract No. NAS8-32703, August 1980.
4. Cheng, A. K., "SSME Alternate Turbopumps Axial Thrust Balance and Secondary Flow Models", Sverdrup Technology MSFC Group, Report No. 322-002-91-153-R01, Contract No. NAS8-37814, October, 1992.
5. Majumdar, A. K. and Van Hooser, K. P., "A General Fluid System Simulation Program to Model Secondary Flows in Turbomachinery", Paper No. AIAA 95-2969, 31st AIAA/ASME/ SAE/ASEE Joint Propulsion Conference, July 10-12, 1995, San Diego, California.
6. Majumdar, A. K., "A Generalized Fluid System Simulation Program to Model Flow Distribution in Fluid Networks", Sverdrup Technology MSFC Group Report No. 331-201-96-003, October 1996. Released to NASA's Computer Software Management and Information Center (COSMIC), The University of Georgia, MFS – 31202, October, 1997.
7. Marsh, M.; Cowan, P., Forbes, J., and Van Hooser, K., "SIMPLEX Turbopump Design", Presented at the 1994 Conference on Advanced Earth-to-Orbit Propulsion Technology, May 17-19, 1994, MSFC.
8. Schallhorn, P.A., Majumdar, A. K., Van Hooser, K. and Marsh, M.: "Flow Simulation in Secondary Flow Passages of a Rocket Engine Turbopump," Paper No. AIAA 98-3684, 34th AIAA/ASME/SAE/ASEE Joint Propulsion Conference, July 13-15, 1998, Cleveland, Ohio.
9. Majumdar, A. K., Bailey, J. W., Schallhorn, P. A. and Steadman, T., "Generalized Fluid System Simulation Program (GFSSP) Version 2.01" Sverdrup Technology MSFC Group Report No. 371-401-98-001, May, 1998, MSFC Science and Engineering Contract NAS 8-40836.